Article

Cell Reports

Dysregulation of miRNA-9 in a Subset of Schizophrenia Patient-Derived Neural Progenitor Cells

Graphical Abstract

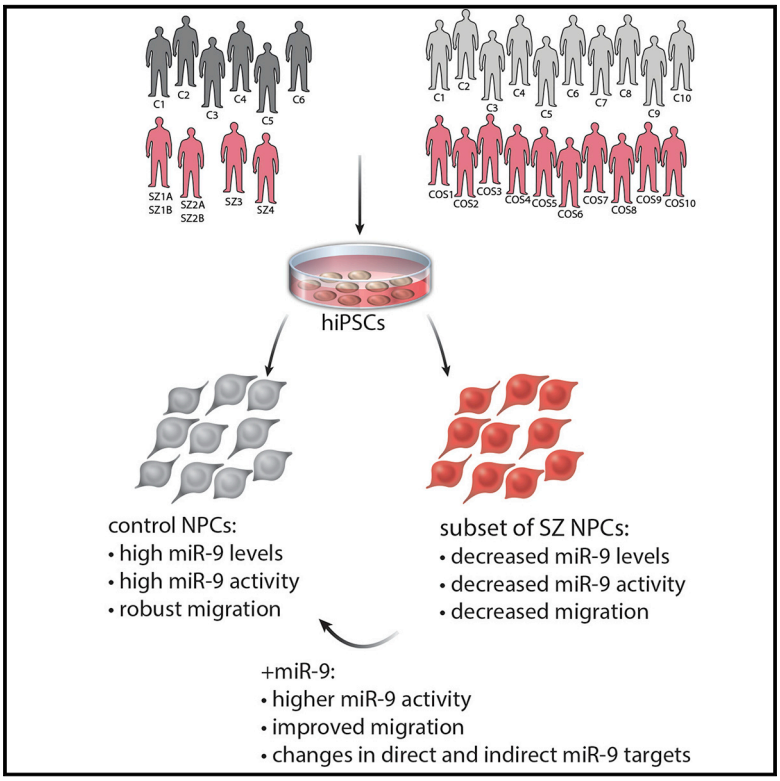

Highlights

- miR-9 is highly expressed in NPCs and downregulated in a subset of SZ NPCs
- miR-9 expression level is strongly correlated with miR-9 regulatory activity
- Manipulation of miR-9 impacts neural migration
- miR-9 effects seem to be mediated by small changes in indirect miR-9 targets

Authors

Aaron Topol, Shijia Zhu, Brigham J. Hartley, ..., David Cotter, Gang Fang, Kristen J. Brennand

Correspondence

gang.fang@mssm.edu (G.F.), kristen.brennand@mssm.edu (K.J.B.)

In Brief

Topol et al. examine the role of decreased miR-9 levels in a subset of schizophrenia patient-derived neural progenitor cells from two independent cohorts. They observe a strong correlation between miR-9 expression and miR-9 regulatory activity. Manipulation of miR-9 impacts neural migration most likely through changes to many indirect miR-9 targets.

Accession Numbers

GSE80163
GSE63738
GSE63734
GSE80170

Topol et al., 2016, Cell Reports *15*, 1024–1036
May 3, 2016 ©2016 The Authors
http://dx.doi.org/10.1016/j.celrep.2016.03.090

OPEN ACCESS
CellPress

Cell Reports
Article

Dysregulation of miRNA-9 in a Subset of Schizophrenia Patient-Derived Neural Progenitor Cells

Aaron Topol,[1,10] Shijia Zhu,[2,10] Brigham J. Hartley,[1,3] Jane English,[4] Mads E. Hauberg,[5,6] Ngoc Tran,[1] Chelsea Ann Rittenhouse,[1] Anthony Simone,[7] Douglas M. Ruderfer,[1] Jessica Johnson,[1] Ben Readhead,[2] Yoav Hadas,[1] Peter A. Gochman,[9] Ying-Chih Wang,[2] Hardik Shah,[2] Gerard Cagney,[8] Judith Rapoport,[9] Fred H. Gage,[7] Joel T. Dudley,[2] Pamela Sklar,[1] Manuel Mattheisen,[5,6] David Cotter,[4] Gang Fang,[2,*] and Kristen J. Brennand[1,3,*]

[1]Department of Psychiatry, Icahn School of Medicine at Mount Sinai, 1425 Madison Avenue, New York, NY 10029, USA
[2]Department of Genetics and Genomic Sciences, Icahn Institute for Genomics and Multiscale Biology, 1425 Madison Avenue, New York, NY 10029, USA
[3]Friedman Brain Institute, Icahn School of Medicine at Mount Sinai, 1425 Madison Avenue, New York, NY 10029, USA
[4]Department of Psychiatry, Royal College of Surgeons in Ireland, Beaumont Hospital, Beaumont, Dublin 9, Ireland
[5]Department of Biomedicine and Centre for Integrative Sequencing (iSEQ), Aarhus University, Wilhelm Meyers Allé 4, Aarhus 8000 C, Denmark
[6]The Lundbeck Foundation Initiative for Integrative Psychiatric Research (iPSYCH), Aarhus University, Wilhelm Meyers Allé 4, Aarhus 8000 C, Denmark
[7]Laboratory of Genetics, Salk Institute for Biological Studies, 10010 North Torrey Pines Road, La Jolla, CA 92037, USA
[8]School of Biomolecular and Biomedical Science, Conway Institute, University College Dublin, Belfield, Dublin 4, Ireland
[9]Childhood Psychiatry Branch, National Institute of Mental Health, National Institutes of Health, Bethesda, MD 20892, USA
[10]Co-first author
*Correspondence: gang.fang@mssm.edu (G.F.), kristen.brennand@mssm.edu (K.J.B.)
http://dx.doi.org/10.1016/j.celrep.2016.03.090

SUMMARY

Converging evidence indicates that microRNAs (miRNAs) may contribute to disease risk for schizophrenia (SZ). We show that microRNA-9 (miR-9) is abundantly expressed in control neural progenitor cells (NPCs) but also significantly downregulated in a subset of SZ NPCs. We observed a strong correlation between miR-9 expression and miR-9 regulatory activity in NPCs as well as between miR-9 levels/activity, neural migration, and diagnosis. Overexpression of miR-9 was sufficient to ameliorate a previously reported neural migration deficit in SZ NPCs, whereas knockdown partially phenocopied aberrant migration in control NPCs. Unexpectedly, proteomic- and RNA sequencing (RNA-seq)-based analysis revealed that these effects were mediated primarily by small changes in expression of indirect miR-9 targets rather than large changes in direct miR-9 targets; these indirect targets are enriched for migration-associated genes. Together, these data indicate that aberrant levels and activity of miR-9 may be one of the many factors that contribute to SZ risk, at least in a subset of patients.

INTRODUCTION

Schizophrenia (SZ) is hypothesized to be a neurodevelopmental condition (Weinberger, 1987) arising from dysregulated development of neural circuitry (Jarskog et al., 2007). Moreover, SZ has a highly heritable component (Schizophrenia Working Group of the Psychiatric Genomics Consortium, 2014), and recent studies have demonstrated that transcripts expressed in the developing prefrontal cortex are enriched for those harboring SZ risk alleles (Gulsuner et al., 2013; Lin et al., 2015), suggesting that disruptions in fetal cortical development may underlie SZ. Multiple lines of strong genetic evidence suggest that microRNAs (miRNAs), particularly miR-137, are involved in the etiology of SZ (Ripke et al., 2011, 2013; Schizophrenia Working Group of the Psychiatric Genomics Consortium, 2014). Additionally, the coding region for a component of miRNA biogenesis, DiGeorge syndrome critical region gene 8 (*DGCR8*), lies within 22q11.2, the most common and penetrant of all recurrently observed SZ-associated copy-number variants (CNVs) (Karayiorgou et al., 2010).

Given that patient human-induced pluripotent stem cell (hiPSC)-derived neural progenitor cells (NPCs) and neurons most resemble fetal brain tissue (Brennand et al., 2015), they are an indispensable tool in the study of possible molecular aspects of SZ predisposition. Using hiPSCs, we previously reported aberrant migration in SZ NPCs (Brennand et al., 2015; Lee et al., 2015) and diminished neuronal connectivity and synaptic activity in SZ neurons (Brennand et al., 2011; Yu et al., 2014), mirroring postmortem pathological findings (Wong and Van Tol, 2003).

Here, we show that miR-9 was not only highly expressed in control NPCs, but also significantly downregulated in a subset of SZ NPCs. We find a correlation between miR-9 expression, miR-9 regulatory activity, and neural migration. Retroviral expression of miR-9 was sufficient to rescue a neural migration deficit in SZ NPCs, whereas knockdown partially phenocopied

aberrant migration in control NPCs. Finally, decreased miR-9 levels were corroborated in a subset of cases from a second and larger cohort comprised of ten cases and ten controls, indicating the robustness of this observation. We posit that dysregulation of miR-9 may contribute to risk for SZ, at least in a subset of patients.

RESULTS

Expression Profile of 800 Annotated miRNAs in SZ NPCs

Unbiased comparison of 800 annotated miRNAs between our previously validated NPCs derived from four SZ patients and six controls (see the Supplemental Experimental Procedures for available clinical information and cell line descriptions) using the Nanostring nCounter expression platform identified hsa-miR-9-5p (miR-9), a regulator of neurogenesis in neural stem cells (Zhao et al., 2009), as the most abundant and the most downregulated miRNA (Bonferroni corrected Student's t test $p < 0.02$) (Figure 1A; Table 1; Table S1), and downregulation was confirmed by qPCR (Figures 1C and S1). Values from independent replicates of the same NPC line for all individuals are indicated by circles (as well as from two independent NPC lines from SZ1 and SZ2), showing that miR-9 levels are consistent between biological samples (Figure 1A). In contrast, miR-137 was not significantly perturbed in SZ NPCs and neurons (Figures 1D and 1E; Tables 1 and 2; Table S1).

This finding was corroborated by a replication hiPSC cohort derived from ten childhood-onset-SZ (COS) patients and ten unrelated controls, all of whom are part of an ongoing longitudinal study conducted at the NIH (see the Supplemental Experimental Procedures for available clinical information). COS patients are thought to represent a subset of adult onset SZ patients defined by onset and severity; at adulthood, there are no genetic or clinical differences between COS patients and those with chronic poor outcome adult onset SZ (see review by Rapoport et al., 2012). Cohort 2 hiPSCs showed normal karyotypes, robust self-renewal, and expression of pluripotency markers (Figures S2A–S2C); two to three validated hiPSC lines were generated per person (see the Supplemental Experimental Procedures for cell line descriptions). Cohort 2 NPCs expressed high levels of NESTIN and SOX2 (Figure S2D). Using Nanostring nCounter analysis, we again observed decreased miR-9 levels in COS NPCs (0.38-fold, $p = 4.6e^{-4}$, nested ANOVA) (Figure 1F; Table S2). Values from biological replicates of NPC lines differentiated from independent hiPSC clones are indicated by circles (C1,2,3,4,8,9,10; COS1,2,3,5,6,7,8,10) as well as independent replicates from the same NPC lines (C2,3,9; COS2,3,4,8) (Figure 1F). Moreover, because the reduced miR-9 level in a subset of SZ NPCs is beyond the inter-individual and intra-individual variations (Figures 1A, 1F, and 1G), we posit that perturbations in miR-9 may be more broadly relevant to SZ and not a result of variability reflected in culture.

Although significantly decreased miR-9 levels were observed on average between SZ and control NPCs across both hiPSC cohorts, miR-9 expression differences were not perfectly correlated with diagnosis. Samples from the two cohorts were combined after adjusting for batch effect with linear regression (see the Experimental Procedures). As shown in Figure 1G, miR-9 levels measured by Nanostring nCounter were significantly lower in SZ NPCs than control NPCs ($p = 1.08e^{-07}$, nested ANOVA). Moreover, we found that miR-9 levels in NPCs derived from all 14 SZ patients were lower than the median in control NPCs ($p = 6.1e^{-05}$, binomial test), and 7 out of 14 SZ NPCs are lower than the 25% quantile of control NPCs ($p = 0.038$, binomial test). These observations indicate that lower miR-9 levels in SZ NPCs relative to control NPCs are largely driven by a significant subset of SZs, which is not unexpected given the heterogeneity of a complex disorder like SZ.

In order to leverage existing datasets, our subsequent mechanistic experiments in this report focused only on our first cohort of NPCs.

miR-9 Targets Enriched for Differentially Expressed Genes in SZ NPCs

In an effort to elucidate miR-9 targets enriched in our previous NPC (GEO: GSE40102) (Brennand et al., 2015) and neuron (GEO: GSE25673) (Brennand et al., 2011) microarray gene expression datasets, we used Partek Genomics Suite, accepting the caveat that the output generated would be a very large list of significant miRNAs (Table S3), likely confounded by the large number of overlaps among putative target genes of different miRNAs (Friedman et al., 2009). Known miR-9 targets were significantly enriched in the differential expression (DE) list (in total 84 miR-9 targets [9.3% of predicted targets] were perturbed [$p < 1e^{-45}$], 56% upregulated, and 44% downregulated) (Table S3).

Global Integrative Modeling Suggests miR-9 Is a Regulator in SZ NPCs

To adjust for overlaps among putative target genes of different miRNAs and to integrate both transcriptional and post-transcriptional regulation of gene expression, we performed global modeling of putative miRNA and transcription factor (TF) targets (Balwierz et al., 2014) with an RNA sequencing (RNA-seq) dataset generated from control and SZ NPCs (GEO: GSE63738) (Topol et al., 2015b) and neurons (GEO: GSE63734) (Table S4). The linear regression-based model was first proposed to predict TF regulatory activities and motifs from yeast gene expression data (Conlon et al., 2003) and further extended to infer the miRNA regulatory activities (Setty et al., 2012). The method regresses the fold change of a gene on its (multiple) putative regulatory miRNAs and TFs (Figures 2A and 2B). The coefficient (Z score) of a miRNA or a TF, estimated using genome-wide fold changes and predicted targets of all miRNAs and TFs, represents the regulatory activity change of the miRNA/TF across all the NPCs. Owing to the inherent properties of a linear regression model, the activity change reflects the non-redundant effect of the miRNA/TF with respect to all the other miRNAs and TFs (Figure 2B). It is worth noting that although putative miRNA/TF targets likely contain false-positive predictions and do not capture cell-type-specific miRNA/TF gene binding, regulatory activities estimated from the regression model are very reliable in general (Balwierz et al., 2014). Refer to the Experimental Procedures for additional details of the model.

Several miRNAs and TFs with significant activity changes were discovered (Figures 2C and 2D; Tables S5 and S6). miR-9 had

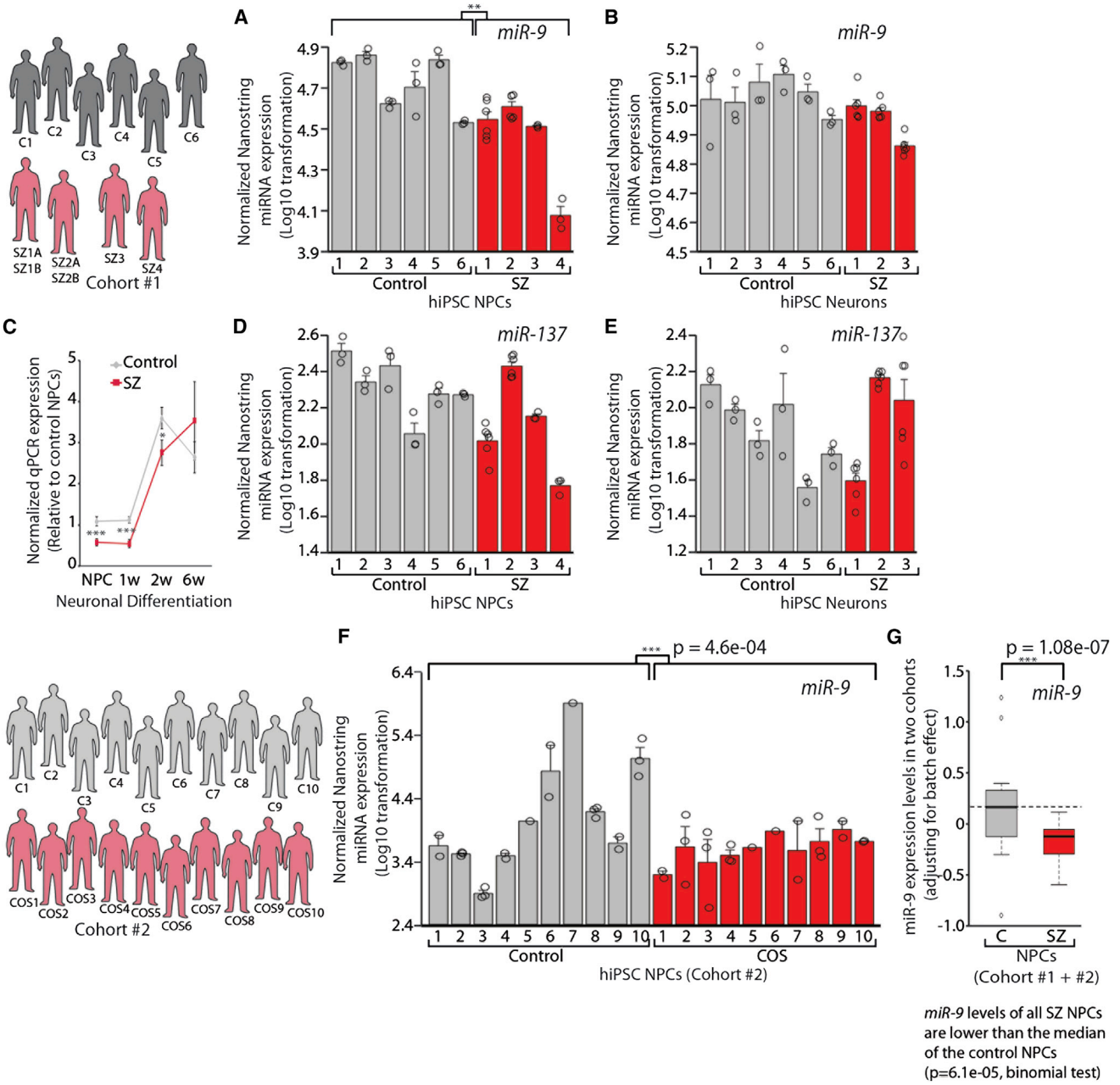

Figure 1. Decreased miR-9 Levels Occur in SZ NPCs but Not SZ hiPSC Neurons

(A, B, D, and E) Nanostring nCounter analysis of normalized miR-9 (A and B) and miR-137 (D and E) expression levels in SZ NPCs (A and D) and neurons (B and E). Values from independent replicates of the same NPC line for all individuals are indicated by circles (as well as from two independent NPC lines from SZ1,2, A and D, and two independent NPC lines from SZ1,2,3, B and E).

(C) qPCR validation of normalized miR-9 expression during the differentiation of SZ NPCs into 1-, 2-, and 6-week-old neurons.

(F) Nanostring nCounter analysis of normalized miR-9 expression levels in NPCs from ten COS patients and ten unrelated controls. Values from biological replicates of NPC lines differentiated from independent hiPSC clones are indicated by circles (C1,2,3,4,8,9,10; COS1,2,3,5,6,7,8,10) as well as independent replicates from the same NPC lines (C2,3,9; COS2,3,4,8).

(G) Samples from two SZ hiPSC NPC cohorts were combined after adjusting for the batch effect with linear regression, where average miR-9 expression level was calculated for each sample. Error bars are SE; *p < 0.05, **p < 0.01, ***p < 0.001.

See also Figures S1 and S2 and Table S2.

Table 1. miRNAs with Highly Significant Perturbations in Expression in SZ hiPSC NPCs

	Abundance	Fold Change (SZ/Control)	Student's t Test	Bonferroni Corrected p Value	Function	Target Genes Perturbed by Microarray	Predicted Activity (*Z* Score)
hsa-miR-98	low	−1.94	$6.0e^{-05}$	0.0479	cancer progression; immune modulation; Alzheimer's disease	yes	1.648
hsa-miR-9-5p	high	−1.70	$2.4e^{-05}$	0.0194	neural differentiation; neural migration; EMT	yes	3.958
hsa-miR-27b-3p	high	−1.69	$5.2e^{-05}$	0.0419	myogenesis; angiogenesis; adipogenesis	yes	0.984
hsa-miR-532-5p	low	−1.66	$4.5e^{-05}$	0.0362	neuronal growth cones; myogenesis	yes	—
hsa-miR-130a-3p	moderate	1.30	$3.5e^{-05}$	0.0279	EMT, hypoxia response; autophagy-lysosomal pathway	yes	1.167

See also Tables S1 and S3.

the greatest activity *Z* score (3.96; Bonferroni corrected p = 0.0032) (Figure 2C; Table 1). For each of the top five miRNAs (Figures 2C and S3A–S3F) and top five TFs identified (Figures 2D and S3G–S3K), we correlated RNA-seq-derived sample-specific activity (Experimental Procedures) to expression levels of miRNAs (from Nanostring nCounter) and TFs (from RNA-seq) in matched samples. Overall, the most significant correlation between miRNA activity and miRNA expression (r = −0.97, p = $1.54e^{-07}$) was observed for miR-9 (Figure 2E). In contrast, miR-137 did not show significant activity change (*Z* = 1.38; p = 0.08, before Bonferroni correction) and showed only a modest correlation between miRNA expression and activity (r = 0.65, p = 0.02) (Figure 2F). REST, a target of miR-9, was observed to have significant activity change among TFs (Figure S3H).

Collectively, multiple analyses suggest that miR-9 may contribute to differential gene expression between SZ and control NPCs. Importantly, our SZ cohort was not selected on the basis of genetic variants at the miR-9 locus; moreover, we identified no broadly shared haplotype in any of the miR-9 loci that would explain these consistent results (see the Supplemental Experimental Procedures for subject rs181900 genotypes). Previously reported CNV genotyping did not detect any specific genetic changes at the miR-9 locus that might be predicted to contribute to SZ risk (Brennand et al., 2011).

Decreased miR-9 Activity Is Specific to SZ NPCs and Not Detected in SZ hiPSC Neurons

When our global integrative analysis was extended to neurons, we observed no substantial miR-9 activity (miR-9 *Z* = 2.40, Bonferroni corrected p = 0.70; miR-137 *Z* = 1.40, Bonferroni corrected p = 1) or correlation between activity and expression (miR-9 r = 0.036, p = 0.92; miR-137 r = 0.64, p = 0.03) in control and SZ hiPSC neurons (Figures 2G and 2H; Tables S5 and S6). Nanostring (Figure 1B; Table 2; Table S1) and qPCR (Figure 1C) analysis confirmed that aberrant miR-9 levels were restricted to SZ NPCs as no significant differences in miR-9 levels were observed between SZ and control hiPSC 6-week-old neurons. Temporal expression profiling of miR-9 expression throughout neuronal differentiation across all four patients and six controls demonstrated significantly decreased miR-9 levels in SZ NPCs and 1-and 2-week-old neurons, which normalized as miR-9 expression increased to control levels over extended neuronal differentiation (Figures 1C and S1), suggesting that the significantly lower expression level of miR-9 in SZ NPCs may not persist in the adult human brain.

Decreased miR-9 Regulatory Activity Correlates to Reduced Migration in SZ NPCs

As stated above, miR-9 regulates neurogenesis and neuronal maturation in vivo (Shibata et al., 2011; Zhao et al., 2009) and plays a role in neural migration in vitro as well (Delaloy et al., 2010). Using neurosphere outgrowth as an assay for neural migration, we have previously shown migration deficits in SZ NPCs (Brennand et al., 2015; Lee et al., 2015) and postulated that decreased miR-9 levels may contribute to this phenotype. We observed a significant positive correlation between radial migration and both endogenous miR-9 activity (p = $3.16e^{-06}$, nested ANOVA) and endogenous miR-9 expression (p = $9.61e^{-06}$, nested ANOVA) in SZ NPC neurospheres (Figure 3A).

Modulating miR-9 Levels Affects Neural Migration

Using a previously characterized retrovirus, RV-MDH-GFP-miR-9 (De Bosscher et al., 2010), hereafter referred to as RV-miR-9-GFP, we increased levels of active miR-9 in control and SZ NPCs (Figure S4A). Comparison of 1,539 neurospheres (375 RV-GFP control, 287 RV-miR-9-GFP control, 416 RV-GFP SZ, and 328 RV-miR-9-GFP SZ) revealed that overexpression of miR-9 in SZ NPCs, but not control NPCs, significantly increased total radial migration (p < 0.0399) (Figures 3B, 3C, and S5; see the Supplemental Experimental Procedures for quantification of the total number of neurospheres analyzed in each assay). In addition to miR-9, we manipulated a second miRNA, miR-137. The miR-137 locus has a well-established and significant genome-wide signal associated with SZ (Ripke et al., 2011, 2013; Schizophrenia Working Group of the Psychiatric Genomics Consortium, 2014) and is brain-enriched with the ability to modulate neural stem cell proliferation and neural differentiation (Smrt et al., 2010; Sun et al., 2011). miR-137 was not significantly differentially expressed between control and SZ NPCs (Figure 1D) or neurons (Figure 1E). Moreover, overexpression of miR-137 using an engineered retrovirus MDH-GFP-miR-137 vector (RV-miR-137-GFP) (Figure S4B) had no apparent effect on the migration of neurospheres derived from SZ patients (p = 0.72) (Figures 3B and 3C) (132 RV-GFP control, 133 RV-miR-137-GFP control, 151 RV-GFP SZ, and 151 RV-miR-137-GFP SZ). Both miR-9 and miR-137 also regulate the replication of

Table 2. miRNAs with Highly Significant Perturbations in Expression in SZ hiPSC Neurons

	Abundance	Fold Change (SZ/Control)	Student's t Test	Bonferroni Corrected p Value	Function	Target Genes Perturbed by Microarray	Predicted Activity (*Z* Score)
hsa-miR-28-5p	moderate	−2.76	$4.2e^{-05}$	0.0337	cellular proliferation	yes	—
hsa-miR-191-5p	high	−2.26	$1.0e^{-05}$	0.0081	spine remodeling in LTP; regulator of BDNF, cancer	no	0.452
hsa-miR-148b-3p	high	−2.22	$1.1e^{-05}$	0.0092	tumor progression	yes	0.664
hsa-miR-1180	high	−2.13	$2.9e^{-06}$	0.0023	unknown	no	—
hsa-miR-450a-5p	moderate	−1.72	$1.5e^{-05}$	0.0122	tumor suppressor	no	—
hsa-let-7d-5p	moderate	−1.70	$6.4e^{-06}$	0.0051	neurogenesis; apoptosis	yes	1.619
hsa-miR-374a-5p	high	−1.52	$1.6e^{-05}$	0.0129	neurogenesis; retinal ganglion cell differentiation	yes	—
hsa-miR-374b-5p	moderate	1.63	$1.5e^{-05}$	0.0118	neurogenesis; retinal ganglion cell differentiation	yes	—
hsa-miR-92a-3p	moderate	1.70	$4.9e^{-06}$	0.0039	neuronal homeostatic scaling; apoptosis; proliferation	yes	1.518
hsa-miR-34a-5p	high	1.81	$5.5e^{-05}$	0.0438	neurite outgrowth; neural migration; memory consolidation	yes	4.157
hsa-miR-30b-5p	moderate	1.85	$5.0e^{-05}$	0.0401	tumor suppressor, stress response	yes	2.527

See also Tables S1 and S3.

NPCs (reviewed in Meza-Sosa et al., 2014); however, we observed only a small insignificant increase in proliferation with RV-miR-9-GFP or RV-miR-137-GFP transduction in either control or SZ hiPSC NPCs using two independent assays (Figures S6A–S6C). Additionally, transient knockdown of miR-9 using locked nucleic acid (LNA) probes in control NPCs significantly decreased total radial migration (166 scrambled control and 154 miR-9-knockdown control) ($p < 0.0009$) (Figures 3D and S5; see the Supplemental Experimental Procedures for quantification of the total number of neurospheres analyzed in each assay).

Effect of Manipulating miR-9 Levels on Global Gene Expression

When we first attempted to quantify changes in ten empirically validated miR-9 target genes (see the Supplemental Experimental Procedures) in control and SZ NPCs stably and efficiently transduced with RV-GFP or RV-miR-9-GFP, we observed that persistent overexpression of miR-9 did not lead to significantly decreased expression of any of these well-characterized candidate miR-9 target genes (Figure S6E; Tables S7 and S8). However, we did detect ameliorated expression of *NRXN1* ($p = 0.0092$), *NRXN2* ($p = 0.0200$), and *NCAM1* ($p = 0.0541$) (Figure S6D; Tables S7 and S8).

To more broadly investigate the effect of manipulating miR-9 levels on miR-9 regulatory activity, we performed transcriptomic profiling to examine global gene expression changes following RV-overexpression of miR-9 in control and SZ NPCs (Figures 4A and 4B). Biological duplicates of passage-matched NPCs from one control (female) and one SZ patient (female) were transduced with either RV-GFP or RV-miR-9-GFP; GFP-positive NPCs were purified by fluorescence-activated cell sorting (FACS) (Figure S4C) and expanded for two passages. In parallel, passage-matched NPCs from two controls (one male, one female) and two SZ patients (one male, one female) were transiently transfected with either scrambled or miR-9 LNA probes. In both instances, miR-9 perturbation was confirmed by qPCR (Figure 4C). Because RV-overexpression was stable and persistent and analyzed after FACS purification and expansion of stable lines, this experiment most likely captured indirect miR-9 targets. Conversely, as miR-9 knockdown was transient and samples were collected within 48 hr, this experiment most likely better reflected direct miR-9 targets. Although RNA-seq analysis revealed large inter-individual heterogeneity, we were able to resolve several functional consistencies in the effects of our miR-9 perturbations: (1) the change in miR-9 activity was consistent with the inhibitory role of miR-9 (Figure 4D), (2) the gene expression fold change of miR-9 target genes (between each perturbation and its corresponding control, summarized by the first principal component; see the Experimental Procedures) was correlated ($r = 0.95$, $p = 3.92e^{-4}$) with miR-9 fold change (Figure 4E), and (3) the differentially expressed (DE) ($p < 0.01$) gene list resulting from miR-9 perturbation (paired t test; see the Experimental Procedures) was enriched for putative miR-9 targets (1.53-fold, $p = 1.2e^{-5}$) (GSE80170).

We integrated the miR-9 perturbation RNA-seq data with our existing RNA-seq datasets contrasting control and SZ hiPSC NPC expression from our cohort 1 (six controls, four patients), to ask whether there was any relationship between the "SZ NPC signature" and "miR-9 perturbation" datasets (Figure 4A; Supplemental Experimental Procedures). Indeed, we observed that the DE (p value < 0.01) in "SZ NPC signature" is enriched for DE (false discovery rate [FDR] <0.01) in "miR-9 perturbation" (the overall enrichment is 2.31-fold [$p = 9.39e^{-9}$]) (Figure 4F); there is significant correlation between DE fold change in these two datasets (overall genes $r = 0.188$; $p < 10e^{-50}$). The significance observed in the above correlation and enrichment analysis between our integrated datasets suggest that perturbation

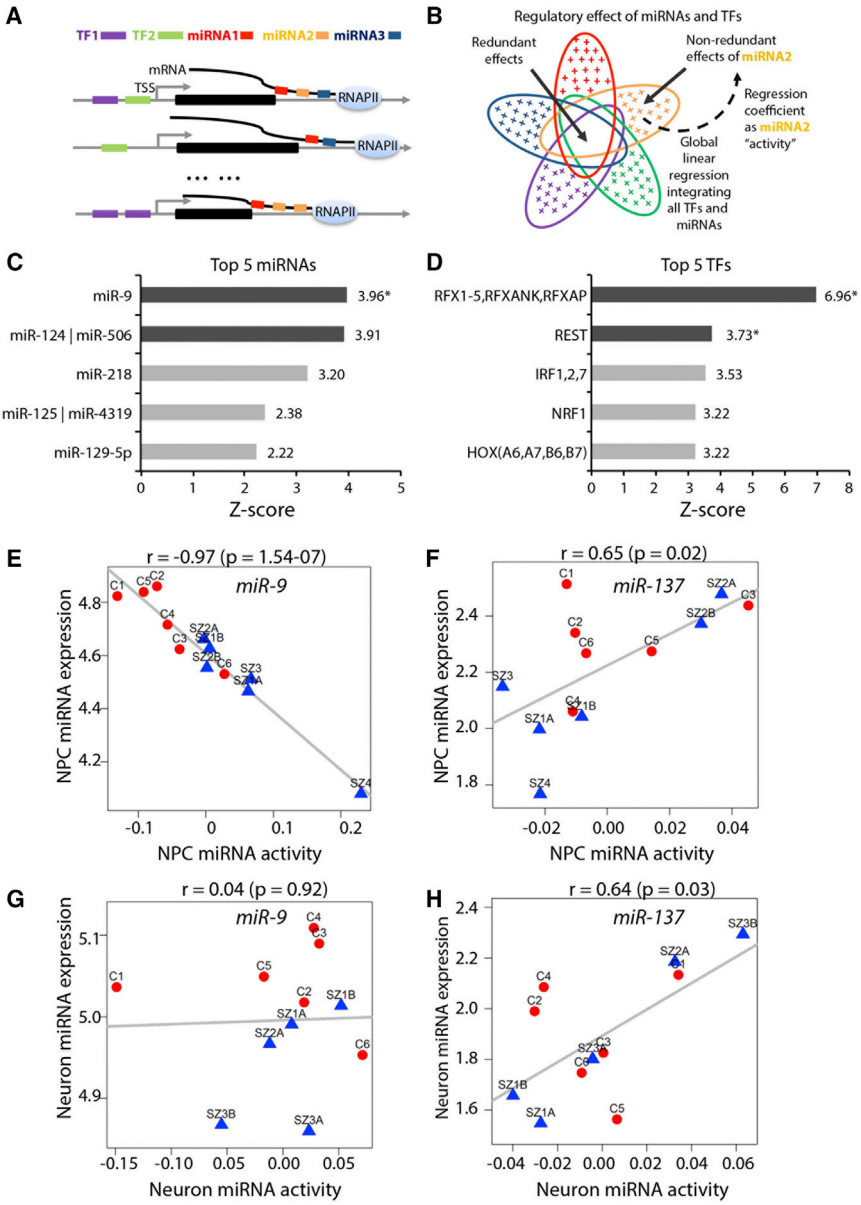

Figure 2. A Global Integrative Model Identified miRNA and Transcription Factor Candidates for Regulating Gene Expression Changes between SZ and Control NPCs

(A) An illustrative example of regulatory relationships between five regulators (two transcription factors [TFs] and three miRNAs, color-coded) and three genes. The expression of each gene can be regulated by one or multiple miRNAs and TFs.

(B) Linear regression is used to model global regulatory relationships between all TFs and miRNAs and genome-wide mRNA expression changes and to predict change of activity of each miRNA and TF across all the samples, conditional on all the other miRNAs and TFs to remove redundant effects, as illustrated for miRNA2. The color codes for miRNAs and TFs are consistent with (A). An ellipse denotes the downstream regulatory effect of a miRNA or a TF. The blank overlapping region denotes the redundant effect shared among miRNAs and TFs; the colored crosses in each ellipse represent the non-redundant regulatory effect for the corresponding miRNA or TF. Each regression coefficient reflects the importance (change of activity) of an miRNA or a TF across all the NPCs.

(C and D) Top five miRNAs (C) and top five TFs (D) with change of activities predicted by the model. The dark gray bars mark miRNAs/TFs with Bonferroni corrected p value < 0.05; the stars mark the miRNAs/TFs whose change of activities are also significantly correlated with their expression.

(E and F) Scatter plots showing relationship between expression and predicted change of activities for miRNA-9 (E) and miR-137 (F) in control and SZ NPCs.

(G and H) Scatter plots show no relationship between expression and predicted change of activities for miRNA-9 (G) and miR-137 (H) in control and SZ hiPSC neurons.

See also Figure S3 and Tables S4, S5, and S6.

of miR-9 partially contributes to the difference between SZ and control NPCs. Among the genes that showed significant changes in the upward direction in both "miR-9 perturbation" and "SZ NPC signature" DE, only three (MTHFD2, MYO1C, and SDC1) are putative miR-9 target genes supported by both TargetScan 6.0 (Friedman et al., 2009) and a published starBase CLIP-seq dataset (Yang et al., 2011), suggesting that few established miR-9 targets are directly being upregulated in low miR-9 conditions (Table S9).

To gain additional mechanistic insight into the migration phenotype under "miR-9 perturbation," we next considered indirect targets. First, we observed that the enrichment of DE genes between the "SZ NPC signature" and "miR-9 perturbation" datasets is focused in the downward direction in low miR-9 conditions (SZ/control and miR-9-knockdown/miR-9-overexpression; 6.43-fold enrichment, p = 5.89e^{-20}), indicating that these are not direct miR-9 targets, which would be expected to be upregulated by miR-9 knockdown (Figure 4F). Second, we found that this enrichment was driven by a subset of the "miR-9 perturbation" dataset: SZ versus SZ-miR-9-overexpression and control-miR-9-knockdown versus control (Figure 4G); this is consistent with the observed changes in migration when manipulating miR-9 levels (Figures 3C and 3D). Third, we identified 37 common genes within the DE of both "miR-9 perturbation" and "SZ NPC signature" (Table S10), putative indirect targets of miR-9. DAVID GO enrichment analysis of this overlapping gene list showed enrichment for plausible migration-associated categories, such as plasma membrane (p value 4.5e^{-05}), cell morphogenesis (p value 2.6e^{-03}), and biological adhesion (p value 1.2e^{-03}) pathways (Figure 4H). Last, but not least, functional modular analysis by weighted gene coexpression network analysis (WGCNA) (Zhang and Horvath, 2005) identified 17 modules among which two were enriched for cell adhesion, extracellular matrix, and membrane part GO terms (Figures 4I and S7).

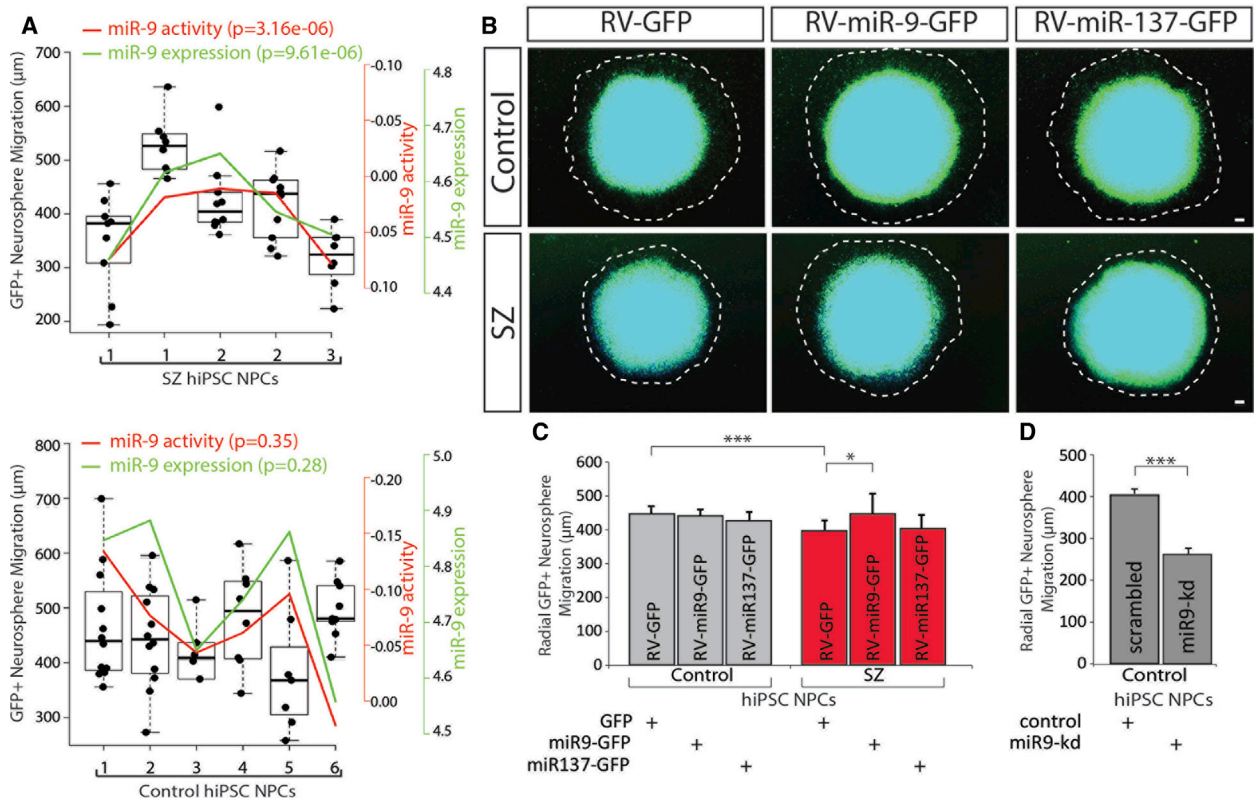

Figure 3. Aberrant Migration in SZ NPCs Rescued by Restoration of miR-9 Levels

(A) Correlation between miR-9 level (both endogenous expression and regulatory activity inferred from RNA-seq data) and radial neurosphere migration in control and SZ NPCs.

(B) Representative fluorescent images of hiPSC forebrain NPC neurosphere outgrowth assay, following stable transduction with RV-GFP, RV-miR-9-GFP, or RV-miR137-GFP. The average distance between the radius of the inner neurosphere (dense aggregate of nuclei) and outer circumference of cells (white dashed line) was calculated. DAPI-stained nuclei (blue). Scale bar, 100 µm.

(C) Radial neurosphere migration by control and SZ NPCs, following stable transduction with RV-GFP, RV-miR-9-GFP, or RV-miR137-GFP.

(D) Radial neurosphere migration by control and SZ NPCs, following transient reduction of miR-9 levels. Error bars are SE; *p < 0.05, **p < 0.01, ***p < 0.001. See also Figures S4, S5, and S6.

Collectively, these analyses reinforce the functional relevance of miR-9 to our observed amelioration of SZ NPC migration and suggest that this cellular phenotype is mediated by a large network of genes that are regulated by miR-9. These data also suggest that miR-9 overexpression in SZ NPCs shifts toward a more control-like NPC signature and miR-9 knockdown in control NPCs shifts toward a more SZ-like NPC signature, at least with respect to migration-related genes and modules.

Because overexpression of miR-9 in SZ NPCs restored only a subset of SZ DEGs, predominantly annotated as migration- and adhesion-related genes, it is important to stress that manipulating miR-9 is not sufficient to achieve a full rescue of the molecular phenotype. Rather, we posit that miR-9 may be one (of the many) post-transcriptional regulator(s) of genes that are perturbed in SZ NPCs.

Effect of Stable miR-9 Overexpression on the Proteome

Although we acknowledge that many miRNAs may act through mRNA-destabilization rather than translational-repression (Guo et al., 2010), we nevertheless conducted an unbiased global proteomic comparison following RV-miR-9 overexpression in control and SZ NPCs, in order to examine whether migration-related DE changes identified from the RNA-seq data could be detected at the protein level. We used label-free mass spectrometry (LC MS/MS) for a quantitative comparison of protein levels across 90 samples, identifying 2,562 proteins across control (one NPC line each derived from six controls) and SZ NPCs (two NPC lines each derived from four SZ patients) stably transduced with either RV-GFP or RV-miR-9-GFP (GFP-positive NPCs were not FACS-purified). Fifty-one proteins were significantly ($p < 0.05$) altered in control miR-9 overexpression NPCs (Table S11) and 45 in SZ miR-9 overexpression NPCs (Table S11), although none remained significant following FDR correction. In both cases, the most perturbed DAVID (http://david.abcc.ncifcrf.gov) pathways included actin cytoskeleton, protein localization, and RNA processing (Tables S12, S13, and S14).

We integrated both the "SZ NPC signature" and "miR-9 perturbation" datasets with our LC MS/MS proteomic data (Figure 5A) to further explore the effects of miR-9 overexpression on indirect miR-9 target genes. First, we observed that proteomic changes

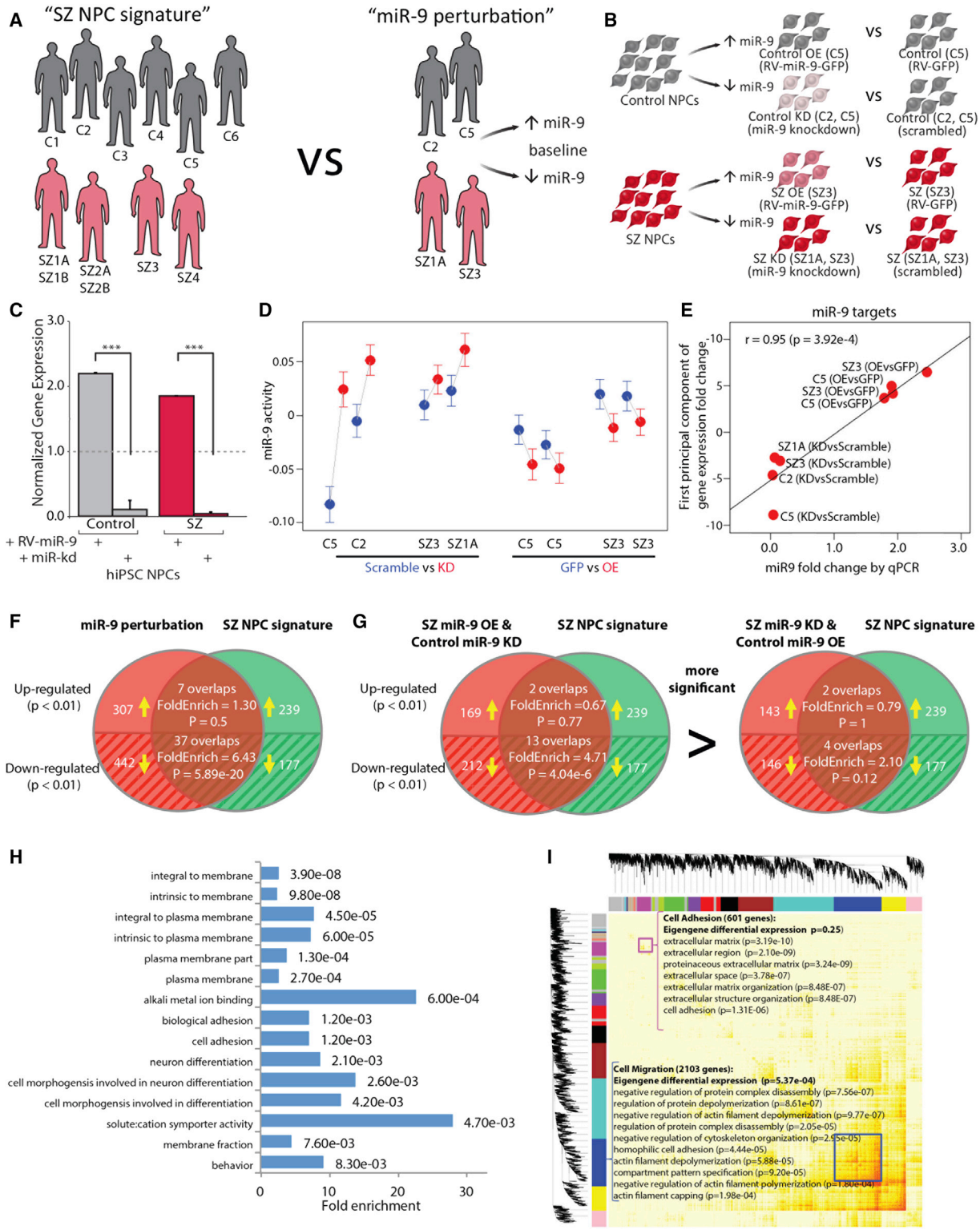

Figure 4. Effect of Manipulating miR-9 Levels on Global Gene Expression

(A) Schematic demonstrating the integration of RNA-seq datasets for "SZ NPC signature" (six controls; four SZ patients) with "miR-9 perturbation" (two controls, two SZ patients).

(B) Experimental design for comparing the effects of stable miR-9 overexpression and transient miR-9 knockdown in control and SZ NPCs.

(legend continued on next page)

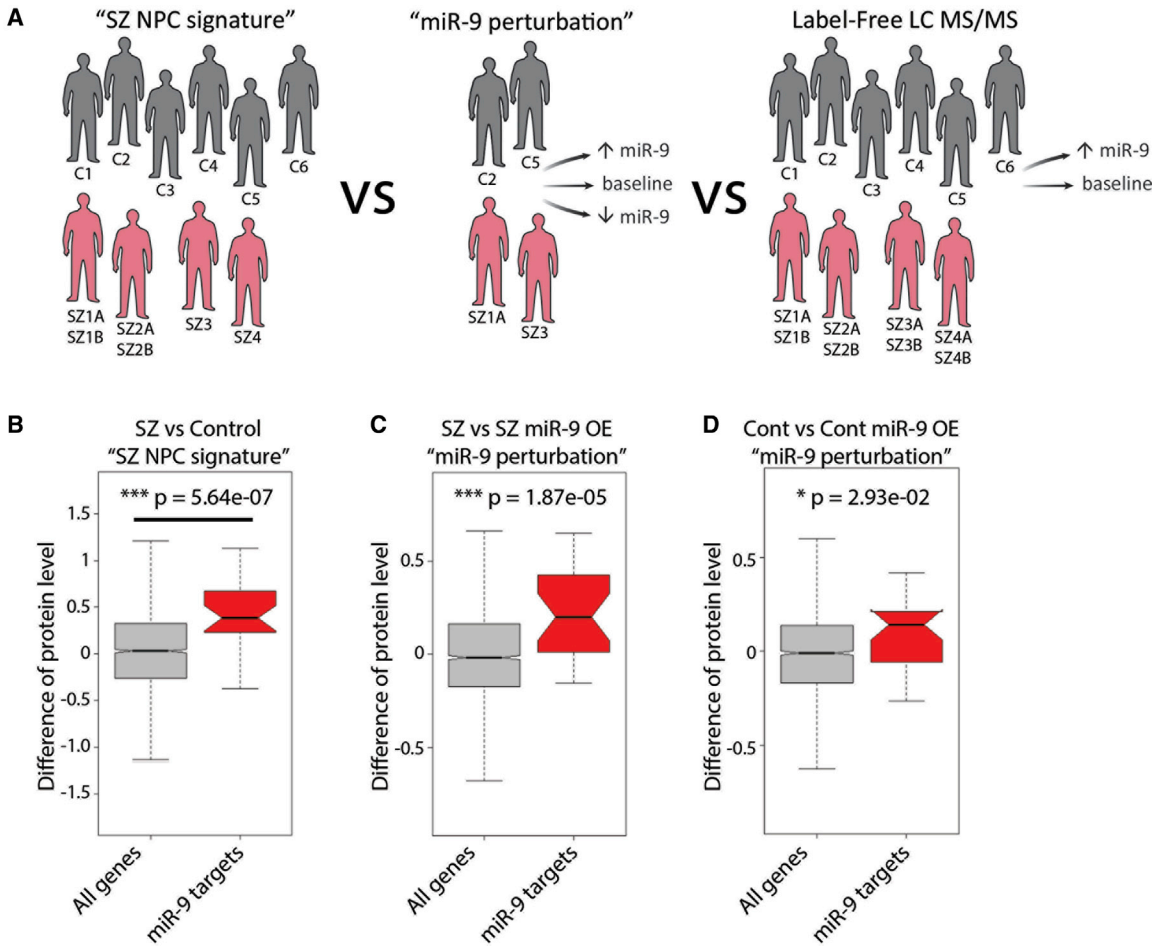

Figure 5. Effect of Manipulating miR-9 Levels on Proteome

(A) Schematic demonstrating integration of "SZ NPC signature" (six controls; four SZ patients) with "miR-9 perturbation" (two controls, two SZ patients) and "label-free LC MS/MS" (six controls; four SZ patients).

(B–D) Putative miR-9 targets enriched for proteomic changes in "SZ NPC signature." The direction of changes were also consistent with the RNA-seq data: significant in both comparisons of SZ/control (B) and SZ+RV-GFP/SZ+RV-miR-9 (C), and modest significant in comparison of control + RV-GFP/control + RV-miR-9 (D).

See also Tables S9, S10, S11, S12, S13, and S14.

were enriched for putative miR-9 targets in each of the "SZ NPC signature" ($p = 5.64e^{-07}$) (Figure 5B), SZ miR-9 overexpression ($p = 1.87e^{-05}$) (Figure 5C), and control miR-9 overexpression ($p = 2.93e^{-02}$) (Figure 5D) RNA-seq datasets (Table S9). Here, the putative miR-9 targets are referred to as the predicted miR-9 targets (based on sequence information from TargetScan) (Friedman et al., 2009) and further filtered by the correlation (negative; $p < 0.01$) between miR-9 and gene expression from our RNA-seq data (SZ versus control hiPSC NPCs). Second, we explored whether the 37 indirect miR-9 target genes identified in the "miR-9 perturbation" dataset also had altered protein levels following miR-9 overexpression; only 9 of these 37 genes were detected, of which five were also changed at the protein level, confirming their potential relevance (Table S10).

(C) qPCR validation of RV-miR-9 overexpression and transient miR-9 knockdown in NPCs.

(D) miR-9 activity for each sample in the perturbation dataset, inferred from RNA-seq data.

(E) Correlation between miR-9 perturbation fold change (validated by qPCR) and miR-9 target gene fold change (first principal component; see the Experimental Procedures).

(F) Overlap between DE genes in the "miR-9 perturbation" dataset and the "SZ NPC signature" RNA-seq datasets.

(G) Overlap between DE genes in two subsets of "miR-9 perturbation" dataset and the "SZ NPC signature" RNA-seq datasets.

(H) DAVID Gene Ontology analysis for the genes significantly differentially expressed in the similar direction between "miR-9 perturbation" and "SZ NPC signature" datasets.

(I) WGCNA for the "miR-9 perturbation" RNA-seq dataset identified 17 modules. Error bars are SE; *$p < 0.05$, **$p < 0.01$, ***$p < 0.001$.

See also Figures S6 and S7 and Tables S7, S8, S9, and S10.

Overall, our global RNA-seq and proteomic analyses of miR-9 perturbations suggest that small changes in direct and indirect miR-9 targets may occur as a result of reduced miR-9 levels in a subset of SZ NPCs.

Genetic Association between miR-9 and SZ

Pre-miR-9 can be transcribed from chromosomes 1 (pre-miR-9-1), 5 (pre-miR-9-2), and 15 (pre-miR-9-3); the mature miRNA sequence generated from all three loci is identical. Although our expression analyses did not distinguish between these immature forms, only pre-miR-9-2 is expressed in neural stem cells differentiated from hiPSCs (Delaloy et al., 2010) and neither miR-9-1 or miR-9-3 show robust expression in the developing human brain; miR-9-2 expression peaks by 16 weeks post-conception (Miller et al., 2014).

Based on a recent genome-wide association study (GWAS) (Hauberg et al., 2016; Schizophrenia Working Group of the Psychiatric Genomics Consortium, 2014), miR-9-2 is near rs181900 (within the r^2 = 0.6 linkage disequilibrium region), a SNP approaching genome-wide significance ($p = 7.1 \times 10^{-8}$) (Hauberg et al., 2016). Moreover, a gene-set enrichment analysis using the summary statistics from PGC2 found an enrichment of predicted miR-9 targets among SZ-associated genes (Hauberg et al., 2016). This suggests that genetic variants in both miR-9 and its targets are associated with increased risk of SZ. Leveraging our "miR-9 perturbation" dataset, which reflects both direct and indirect miR-9 targets, we performed an integrative competitive gene-set enrichment analysis (Hauberg et al., 2016) (see the Supplemental Experimental Procedures) with the PGC2 GWAS summary statistics (Schizophrenia Working Group of the Psychiatric Genomics Consortium, 2014). We observed that the "miR-9 perturbation" DE list was enriched for genes associated with SZ ($p = 7.46 \times 10^{-4}$). Furthermore, focusing specifically on indirect miR-9 targets (those genes in the "miR-9 perturbation" DE list that were not in the TargetScan list of predicted miR-9 targets) also revealed enrichment among genes associated with SZ (p = 0.0020). Together, both our NPC-derived data and the integrative GWAS analysis support the link between miR-9 and SZ.

DISCUSSION

Using unbiased miRNA expression analysis, we report decreased miR-9 levels in a subset of SZ NPCs from two independent SZ patient cohorts (totaling 14 SZ patients and 16 controls) reprogrammed and differentiated independently and using different methodologies. We observed a strong correlation between miR-9 expression and miR-9 regulatory activity in NPCs as well as between miR-9 levels/activity, neural migration, and diagnosis. Although, in comparison to GWAS, the sample sizes achievable in hiPSC studies remain small, our findings suggest that aberrant levels and activity of miR-9 may be one of the many factors that contribute to SZ risk, at least in a subset of patients. All SZ NPCs (16 individuals) had reduced miR-9 levels relative to the median value of control NPCs. We further defined a subset (50%) of the SZ NPCs (using the 25% quantile of the control NPCs) that seem to be driving the signal of decreased miR-9 levels. Of course, owing to the sample sizes involved, these findings must necessarily be considered preliminary until they can be confirmed in much larger hiPSC and/or post-mortem cohorts.

Because rs181900 genotype does not explain differences in miR-9 levels and activity in our SZ NPCs (see the Supplemental Experimental Procedures for subject rs181900 genotypes), we posit that there may be both miR-9 genotype- and non-genotype-dependent changes in the miR-9-controlled regulatory network that affect SZ risk in a subset of patients; one or more SZ risk factors may act either upstream or downstream of miR-9. If the impact of these genetic variations is indeed during early cortical development, this would be consistent with our inability to detect perturbed miR-9 levels in post-mortem DLPFC obtained from ten SZ patients and ten controls (Figure S1E), as well as array-based miRNA studies of the Stanley Brain Bank, which found no significant difference in miR-9 expression levels in post-mortem cortical tissue from 38 controls and 37 SZ patients (Miller et al., 2012; Perkins et al., 2007).

Interestingly, we found that manipulating miR-9 levels resulted in small changes in the transcript and protein levels of many genes, many of which are not predicted to be direct miR-9 targets. This is consistent with a recent RNA-seq dataset generated by overexpressing miR-137 in human neural stem cells (Collins et al., 2014) and other reports that perturbations in miRNAs tend to yield only subtle changes, but in many genes (Guo et al., 2010). The stronger correlation of miR-9 expression, activity, and migration in SZ NPCs than in control NPCs was unexpected and may imply that the genetic (or epigenetic) background of SZ patients has epistasis with miR-9 activity, reflecting genetic polymorphisms or perturbations in expression networks prevalent in SZ. These findings support a model of an extremely complex genetic architecture underlying SZ risk, one in which miR-9 is just one of many factors contributing to SZ predisposition in a subset of patients. In line with this hypothesis, our gene-set enrichment analyses using the PGC2 GWAS showed that both direct and indirect targets of miR-9 are enriched for SZ risk loci. Given our findings of reduced miR-9 levels in a subset of SZ patients, it is important to consider whether genetic and/or clinical characteristics (such as various research domain criteria [RDoC]) correlate to miR-9 status. More broadly, a future question for investigation will concern the extent to which miR-9 dysregulation occurs in larger hiPSC cohorts generated from SZ, bipolar disorder and autism spectrum disorder patients.

Although hiPSC-based RNA-seq studies have small sample sizes, the computational methods used in our study demonstrate that integrative analysis leveraging the rich and increasing collection of miRNA targets and transcription factor targets have great power and specificity to predict regulators. We expect the general computational and integrative methodology presented in this study to have broader impact in studies of other diseases using hiPSCs.

EXPERIMENTAL PROCEDURES

Description of SZ Patients, hiPSC Reprogramming, and NPC Differentiation

See the Supplemental Experimental Procedures for available clinical information and cell line descriptions.

For cohort 1, patient and control NPCs were differentiated from hiPSCs reprogrammed from fibroblasts obtained from Coriell or ATCC. In total, NPCs from four patients and six controls were compared, as described previously (Brennand et al., 2011, 2015). A summary of cohort 1 NPC lines used in each assay can be found in the Supplemental Experimental Procedures.

For cohort 2, fibroblast biopsies were obtained from patients with childhood-onset-SZ (COS) and unrelated controls that were recruited as part of a longitudinal study by Dr. Judith Rapoport (NIMH). hiPSCs were derived via sendal viral reprogramming methods as described previously (Lee et al., 2015).Cohort 2 COS NPCs were generated in a similar method to cohort 1 (Brennand et al., 2011, 2015), although differentiated with dual-SMAD inhibition (Chambers et al., 2009) to improve yield, as described (Topol et al., 2015a); five controls from cohort 2 were published previously (Lee et al., 2015). NPCs were maintained at high density, grown on Matrigel in NPC media (DMEM/F12, 1× N2, 1× B27-RA [Invitrogen], 1 μg/ml Laminin [Invitrogen], and 20 ng/ml FGF2 [Invitrogen]) and split ~1:3–1:4 every week with Accutase (Millipore) (Brennand et al., 2011). Detailed description can be found in the Supplemental Experimental Procedures.

All work was reviewed by the Internal Review Board of the Icahn School of Medicine at Mount Sinai. This work was also reviewed by the Embryonic Stem Cell Research Oversight Committee at the Icahn School of Medicine at Mount Sinai.

Gene and miRNA Expression Analysis

Gene expression analysis was performed on passage-matched NPCs cultured on Matrigel (see the Supplemental Experimental Procedures for cell line and passage information). For SZ signature, NPCs or neurons were lysed in RNA BEE (Tel-test). RNA was chloroform extracted, pelleted with isopropanol, washed with 70% ethanol, and resuspended in water. RNA was treated with RQ1 RNase-free DNase (Promega) for 30 min at 37°C and then the reaction was inactivated by incubation with EGTA Stop buffer at 65°C for 10 min. Total RNA for RNA-seq was purified using the miRNeasy Mini Kit (QIAGEN). For miR-9 perturbation, total RNA was purified with the miRNeasy Mini Kit (Qiagen), treated on the column with RNAse-free DNAse Kit (Qiagen), and eluted in water.

For RNA-seq, samples were prepared and run by the Genomics Core at Icahn School of Medicine at Mount Sinai. The Illumina HiSeq 2500 RNA kit was used for 100 nt/single end reads, four samples were run per lane. Raw cDNA reads were aligned to the hg19 reference with the spliced gap aligner STAR, with count-based quantitation carried out via the Subread package featureCounts at the gene level for UCSC annotation build. The count data were normalized and modeled as over-dispersed Poisson data using a negative binomial model in the Bioconductor package edgeR (Robinson et al., 2010). Fold changes, p values, and false discovery rates (FDRs) are obtained from the same package for integrative analysis.

For Nanostring miRNA studies, we used nCounter Human v2 miRNA (NS_H_MIR_V2.1) (based on miRBase v18). The public R package "NanoStringNorm" was used to select the best normalization method for Nanostring miRNA expression based on the consistency between technical replicates (Waggott et al., 2012). When combining the two SZ cohorts, we regressed away the batch effect with a simple regression model and used residuals as the miR9 expression.

Global Integrative Modeling of miRNAs, TFs, and Differential Gene Expression

The regression model is defined as: $f_g = \sum_i A_i M_{ig} + \sum_j B_j N_{jg} + C$, where f_g is the fold change of gene g between two conditions; M_{ig} is the number of binding sites of miRNA i on the 3′ UTR of the gene g; N_{jg} is the number of binding sites of TF j on the promoter of gene g; and A, B, and C (a constant) can be inferred based on the values of f, M, and N for all the genes in the RNA-seq data. The Z scores of coefficients A_i and B_j represent the activity changes of miRNA i and TF j, respectively. Global miRNA binding sites represented by 86 miRNA seed families are based on TargetScan 6.0 (Friedman et al., 2009). Global TF binding sites represented by 190 position-weighted matrices (PWMs) covering 350 mammalian TFs were based on the union of JASPAR (Sandelin et al., 2004), TRANSFAC (Matys et al., 2003), and additional motifs from chromatin immunoprecipitation with DNA microarray and chromatin immunoprecipitation sequencing (ChIP-seq) data collected by Balwierz et al. (2014). The initial regression analysis was done using ISMARA (Balwierz et al., 2014) before further integrative analysis with miRNA expression data; sample-specific miRNA/TF activity was estimated by the same regression model where the fold changes were calculated between a single sample and all the samples combined together. These sample-specific miRNA/TF activities were correlated with miRNA/TF expressions for the matched sample as presented in the main text.

Overexpression of miR-9

The human miR-9-3 gene was previously amplified by PCR from normal genomic DNA and cloned into the MDH1-PGK-GFP 2.0 retroviral vector (http://www.addgene.org/25036) (De Bosscher et al., 2010). We similarly amplified and cloned human miR-137 into the MDH1-PGK-GFP 2.0 retroviral vector. High-titer retroviral supernatant was generated by co-transfection of miRNA expression vector together with PUMVC (http://www.addgene.org/8449/) and CMV-VSVG to package retrovirus in HEK293T cells.

Knockdown of miR-9

hiPSC-derived NPCs were transiently transfected with miRCURY LNA knockdown probes (Exiqon) with Lipofectamine RNAiMAX (Life Technology) in Optimem (ThermoFisher Scientific) for 24 hr. A scrambled miRNA, which bears no homology to any known miRNA or mRNA sequences in human, mouse, and rat, was used as negative control, and hsa-anti-miR-9 (410014-08) (100 nM) was used to specifically inhibit miR-9. Twenty-four hours after transfection, NPCs were dissociated with Accutase in order to generate neurospheres. Neurospheres were additionally cultured in miRCURY LNA knockdown probes (Exiqon) with Lipofectamine RNAiMAX (Life Technology) in NPC media.

Neurosphere Migration Assay

Forty-eight hour radial neurosphere migration was assayed as previously described (Brennand et al., 2015; Lee et al., 2015). A quantification of the total number of neurospheres analyzed in each assay can be found in the Supplemental Experimental Procedures. Detailed descriptions can be found in the Supplemental Experimental Procedures.

LC MS/MS Quantitative Mass Spectrometry

To compare global protein levels in control and SZ NPCs (stably transduced with RV-GFP or RV-miR-9-GFP), we used quantitative label-free LC-MS/MS analysis. We injected 2 μg of protein from each control (one NPC line each derived from six controls) and SZ (two NPC lines each derived from four SZ patients) hiPSC forebrain NPC line, in triplicate, on a Thermo Q-Exactive mass spectrometer equipped with a Dionex Ultimate 3000 (RSLCnano) chromatography system. Detailed description can be found in the Supplemental Experimental Procedures.

Statistical Analysis

For phenotypic and qPCR analysis, statistical analysis was performed using JMP. Box-Cox transformation of raw data was performed to correct non-normal distribution of the data and residuals. Improvements were assessed by Shapiro-Wilk W test of the transformed data and residuals. Means were compared within diagnosis by one-way analysis using both Student's t test and Tukey-Kramer honest significant difference (HSD). Finally, a nested analysis of values for individual patients was performed using standard least-squares analysis comparing means for all pairs using Student's t test for specific pairs and Tukey-Kramer HSD for multiple comparisons. Student's t tests were used to test statistical differences between control and SZ Nanostring and LC MS/MS analyses, with subsequent correction for multiple hypotheses done by Bonferroni and/or Benjamini-Hochberg methods, as noted. In all figures, data presented are from a single representative experimental replicate where pooled data represent biological replicate samples within a given experiment. Error bars represent SE. *$p < 0.05$, **$p < 0.01$, ***$p < 0.001$.

ACCESSION NUMBERS

The RNA-seq data reported in this paper is part of GEO superseries GSE80163. The accession numbers for the RNA-seq data for control and SZ NPCs and

neurons are GSE63738 and GSE63734, respectively. The accession number for the miR-9 perturbation RNA-seq data is GSE80170.

SUPPLEMENTAL INFORMATION

Supplemental Information includes Supplemental Experimental Procedures and seven figures and 14 tables and can be found with this article online at http://dx.doi.org/10.1016/j.celrep.2016.03.090.

AUTHOR CONTRIBUTIONS

A.T. contributed to experimental design and completed the NPC experiments. S.Z. analyzed all RNA-seq data, Nanostring nCounter data, proteomic data, and completed miRNA functional activity modeling assisted by Y.-C.W. and H.S., who performed the RNA-seq read alignment. B.J.H. differentiated and validated COS and control NPCs; P.A.G. and J.R. contributed COS and control fibroblasts. C.R. and N.T. assisted with analysis of the replication and neurosphere migration experiments. J.E., G.C., and D.C. completed the mass spectrometry experiments. M.E.H. and M.M. integrated findings into the PGC2 GWAS. A.S. identified the first differences in miR-9 levels in SZ NPCs with K.J.B. and F.H.G. Y.H. contributed to qPCR. D.R., J.J., and P.S. genotyped the SZ patients included in this study. B.R. and J.D. performed a drug enrichment analysis. G.F. and K.J.B. designed the experiments, supervised data analysis, and wrote the manuscript.

ACKNOWLEDGMENTS

K.J.B. is a New York Stem Cell Foundation-Robertson Investigator. The K.J.B. lab is supported by the Brain and Behavior Research Foundation, NIH grants R01 MH101454 and R01 MH106056, and the New York Stem Cell Foundation. The G.F. lab is supported by NIH grants R01 MH097276 and R01 GM114472. The D.C. lab is supported by Health Research Board Clinical Scientist Award. FACS purification was conducted at the ISMMS Flow Cytometry Center of Research Excellence, and RNA-seq was conducted at the ISMMS Genomics Core Facility. This work was supported in part through the computational resources and staff expertise provided by the Department of Scientific Computing at the Icahn School of Medicine at Mount Sinai. As per our agreement with Coriell Cell Repository, some hiPSC lines generated from control and SZ fibroblasts will be available from Coriell. Additionally, all control, SZ, and COS hiPSCs are currently being deposited with the NIMH Center for Collaborative Studies of Mental Disorders at RUCDR.

Received: December 21, 2015
Revised: March 2, 2016
Accepted: March 27, 2016
Published: April 21, 2016

REFERENCES

Balwierz, P.J., Pachkov, M., Arnold, P., Gruber, A.J., Zavolan, M., and van Nimwegen, E. (2014). ISMARA: automated modeling of genomic signals as a democracy of regulatory motifs. Genome Res. *24*, 869–884.

Brennand, K.J., Simone, A., Jou, J., Gelboin-Burkhart, C., Tran, N., Sangar, S., Li, Y., Mu, Y., Chen, G., Yu, D., et al. (2011). Modelling schizophrenia using human induced pluripotent stem cells. Nature *473*, 221–225.

Brennand, K., Savas, J.N., Kim, Y., Tran, N., Simone, A., Hashimoto-Torii, K., Beaumont, K.G., Kim, H.J., Topol, A., Ladran, I., et al. (2015). Phenotypic differences in hiPSC NPCs derived from patients with schizophrenia. Mol. Psychiatry *20*, 361–368.

Chambers, S.M., Fasano, C.A., Papapetrou, E.P., Tomishima, M., Sadelain, M., and Studer, L. (2009). Highly efficient neural conversion of human ES and iPS cells by dual inhibition of SMAD signaling. Nat. Biotechnol. *27*, 275–280.

Collins, A.L., Kim, Y., Bloom, R.J., Kelada, S.N., Sethupathy, P., and Sullivan, P.F. (2014). Transcriptional targets of the schizophrenia risk gene MIR137. Transl. Psychiatry *4*, e404.

Conlon, E.M., Liu, X.S., Lieb, J.D., and Liu, J.S. (2003). Integrating regulatory motif discovery and genome-wide expression analysis. Proc. Natl. Acad. Sci. USA *100*, 3339–3344.

De Bosscher, K., Haegeman, G., and Elewaut, D. (2010). Targeting inflammation using selective glucocorticoid receptor modulators. Curr. Opin. Pharmacol. *10*, 497–504.

Delaloy, C., Liu, L., Lee, J.A., Su, H., Shen, F., Yang, G.Y., Young, W.L., Ivey, K.N., and Gao, F.B. (2010). MicroRNA-9 coordinates proliferation and migration of human embryonic stem cell-derived neural progenitors. Cell Stem Cell *6*, 323–335.

Friedman, R.C., Farh, K.K.-H., Burge, C.B., and Bartel, D.P. (2009). Most mammalian mRNAs are conserved targets of microRNAs. Genome Res. *19*, 92–105.

Gulsuner, S., Walsh, T., Watts, A.C., Lee, M.K., Thornton, A.M., Casadei, S., Rippey, C., Shahin, H., Nimgaonkar, V.L., Go, R.C., et al.; Consortium on the Genetics of Schizophrenia (COGS); PAARTNERS Study Group (2013). Spatial and temporal mapping of de novo mutations in schizophrenia to a fetal prefrontal cortical network. Cell *154*, 518–529.

Guo, H., Ingolia, N.T., Weissman, J.S., and Bartel, D.P. (2010). Mammalian microRNAs predominantly act to decrease target mRNA levels. Nature *466*, 835–840.

Hauberg, M.E., Roussos, P., Grove, J., Borglum, A.D., and Mattheisen, M.; Schizophrenia Working Group of the Psychiatric Genomics Consortium (2016). Analyzing the role of microRNAs in schizophrenia in the context of common genetic risk variants. JAMA Psychiatry, Published online March 9, 2016. http://dx.doi.org/10.1001/jamapsychiatry.2015.3018.

Jarskog, L.F., Miyamoto, S., and Lieberman, J.A. (2007). Schizophrenia: new pathological insights and therapies. Annu. Rev. Med. *58*, 49–61.

Karayiorgou, M., Simon, T.J., and Gogos, J.A. (2010). 22q11.2 microdeletions: linking DNA structural variation to brain dysfunction and schizophrenia. Nat. Rev. Neurosci. *11*, 402–416.

Lee, I.S., Carvalho, C.M.B., Douvaras, P., Ho, S.M., Hartley, B.J., Zuccherato, L.W., Ladran, I.G., Siegel, A.J., McCarthy, S., Malhotra, D., et al. (2015). Characterization of molecular and cellular phenotypes associated with a heterozygous CNTNAP2 deletion using patient-derived hiPSC neural cells. NPJ Schizophr *1*, 15019.

Lin, G.N., Corominas, R., Lemmens, I., Yang, X., Tavernier, J., Hill, D.E., Vidal, M., Sebat, J., and Iakoucheva, L.M. (2015). Spatiotemporal 16p11.2 protein network implicates cortical late mid-fetal brain development and KCTD13-Cul3-RhoA pathway in psychiatric diseases. Neuron *85*, 742–754.

Matys, V., Fricke, E., Geffers, R., Gössling, E., Haubrock, M., Hehl, R., Hornischer, K., Karas, D., Kel, A.E., Kel-Margoulis, O.V., et al. (2003). TRANSFAC: transcriptional regulation, from patterns to profiles. Nucleic Acids Res. *31*, 374–378.

Meza-Sosa, K.F., Pedraza-Alva, G., and Pérez-Martínez, L. (2014). microRNAs: key triggers of neuronal cell fate. Front. Cell. Neurosci. *8*, 175.

Miller, B.H., Zeier, Z., Xi, L., Lanz, T.A., Deng, S., Strathmann, J., Willoughby, D., Kenny, P.J., Elsworth, J.D., Lawrence, M.S., et al. (2012). MicroRNA-132 dysregulation in schizophrenia has implications for both neurodevelopment and adult brain function. Proc. Natl. Acad. Sci. USA *109*, 3125–3130.

Miller, J.A., Ding, S.L., Sunkin, S.M., Smith, K.A., Ng, L., Szafer, A., Ebbert, A., Riley, Z.L., Royall, J.J., Aiona, K., et al. (2014). Transcriptional landscape of the prenatal human brain. Nature *508*, 199–206.

Perkins, D.O., Jeffries, C.D., Jarskog, L.F., Thomson, J.M., Woods, K., Newman, M.A., Parker, J.S., Jin, J., and Hammond, S.M. (2007). microRNA expression in the prefrontal cortex of individuals with schizophrenia and schizoaffective disorder. Genome Biol. *8*, R27.

Rapoport, J.L., Giedd, J.N., and Gogtay, N. (2012). Neurodevelopmental model of schizophrenia: update 2012. Mol. Psychiatry *17*, 1228–1238.

Ripke, S., Sanders, A.R., Kendler, K.S., Levinson, D.F., Sklar, P., Holmans, P.A., Lin, D.Y., Duan, J., Ophoff, R.A., Andreassen, O.A., et al.; Schizophrenia Psychiatric Genome-Wide Association Study (GWAS) Consortium (2011).

Genome-wide association study identifies five new schizophrenia loci. Nat. Genet. *43*, 969–976.

Ripke, S., O'Dushlaine, C., Chambert, K., Moran, J.L., Kähler, A.K., Akterin, S., Bergen, S.E., Collins, A.L., Crowley, J.J., Fromer, M., et al.; Multicenter Genetic Studies of Schizophrenia Consortium; Psychosis Endophenotypes International Consortium; Wellcome Trust Case Control Consortium 2 (2013). Genome-wide association analysis identifies 13 new risk loci for schizophrenia. Nat. Genet. *45*, 1150–1159.

Robinson, M.D., McCarthy, D.J., and Smyth, G.K. (2010). edgeR: a Bioconductor package for differential expression analysis of digital gene expression data. Bioinformatics *26*, 139–140.

Sandelin, A., Alkema, W., Engström, P., Wasserman, W.W., and Lenhard, B. (2004). JASPAR: an open-access database for eukaryotic transcription factor binding profiles. Nucleic Acids Res. *32*, D91–D94.

Schizophrenia Working Group of the Psychiatric Genomics Consortium (2014). Biological insights from 108 schizophrenia-associated genetic loci. Nature *511*, 421–427.

Setty, M., Helmy, K., Khan, A.A., Silber, J., Arvey, A., Neezen, F., Agius, P., Huse, J.T., Holland, E.C., and Leslie, C.S. (2012). Inferring transcriptional and microRNA-mediated regulatory programs in glioblastoma. Mol. Syst. Biol. *8*, 605.

Shibata, M., Nakao, H., Kiyonari, H., Abe, T., and Aizawa, S. (2011). MicroRNA-9 regulates neurogenesis in mouse telencephalon by targeting multiple transcription factors. J. Neurosci. *31*, 3407–3422.

Smrt, R.D., Szulwach, K.E., Pfeiffer, R.L., Li, X., Guo, W., Pathania, M., Teng, Z.Q., Luo, Y., Peng, J., Bordey, A., et al. (2010). MicroRNA miR-137 regulates neuronal maturation by targeting ubiquitin ligase mind bomb-1. Stem Cells *28*, 1060–1070.

Sun, G., Ye, P., Murai, K., Lang, M.F., Li, S., Zhang, H., Li, W., Fu, C., Yin, J., Wang, A., et al. (2011). miR-137 forms a regulatory loop with nuclear receptor TLX and LSD1 in neural stem cells. Nat. Commun. *2*, 529.

Topol, A., Tran, N.N., and Brennand, K.J. (2015a). A guide to generating and using hiPSC derived NPCs for the study of neurological diseases. J. Vis. Exp. *96*, e52495.

Topol, A., Zhu, S., Tran, N., Simone, A., Fang, G., and Brennand, K.J. (2015b). Altered WNT signaling in human induced pluripotent stem cell neural progenitor cells derived from four schizophrenia patients. Biol. Psychiatry *78*, e29–e34.

Waggott, D., Chu, K., Yin, S., Wouters, B.G., Liu, F.F., and Boutros, P.C. (2012). NanoStringNorm: an extensible R package for the pre-processing of NanoString mRNA and miRNA data. Bioinformatics *28*, 1546–1548.

Weinberger, D.R. (1987). Implications of normal brain development for the pathogenesis of schizophrenia. Arch. Gen. Psychiatry *44*, 660–669.

Wong, A.H., and Van Tol, H.H. (2003). Schizophrenia: from phenomenology to neurobiology. Neurosci. Biobehav. Rev. *27*, 269–306.

Yang, J.H., Li, J.H., Shao, P., Zhou, H., Chen, Y.Q., and Qu, L.H. (2011). starBase: a database for exploring microRNA-mRNA interaction maps from Argonaute CLIP-Seq and Degradome-Seq data. Nucleic Acids Res. *39*, D202–D209.

Yu, D.X., Di Giorgio, F.P., Yao, J., Marchetto, M.C., Brennand, K., Wright, R., Mei, A., McHenry, L., Lisuk, D., Grasmick, J.M., et al. (2014). Modeling hippocampal neurogenesis using human pluripotent stem cells. Stem Cell Reports *2*, 295–310.

Zhang, B., and Horvath, S. (2005). A general framework for weighted gene co-expression network analysis. Stat. Appl. Genet. Mol. Biol. *4*, e17.

Zhao, C., Sun, G., Li, S., and Shi, Y. (2009). A feedback regulatory loop involving microRNA-9 and nuclear receptor TLX in neural stem cell fate determination. Nat. Struct. Mol. Biol. *16*, 365–371.